Research Article | Vol. 25, No. 7 | 3 Apr 2017 | OPTICS EXPRESS 7884

Optics EXPRESS

# Size-optimized polymeric whispering gallery mode lasers with enhanced sensing performance

SARAH KRÄMMER,[1,*] SANAZ RASTJOO,[1] TOBIAS SIEGLE,[1] SENTAYEHU F. WONDIMU,[2,3] CAROLIN KLUSMANN,[1] CHRISTIAN KOOS,[2,3] AND HEINZ KALT[1]

[1]*Institute of Applied Physics (APH), Karlsruhe Institute of Technology (KIT), Wolfgang-Gaede-Str. 1, 76131 Karlsruhe, Germany*
[2]*Institute of Microstructure Technology (IMT), Karlsruhe Institute of Technology (KIT), Hermann-von-Helmholtz-Platz 1, 76344 Eggenstein-Leopoldshafen, Germany*
[3]*Institute of Photonics and Quantum Electronics (IPQ), Karlsruhe Institute of Technology (KIT), Kaiserstrasse 12, 76131 Karlsruhe, Germany*
[*]*sarah.kraemmer@kit.edu*

**Abstract:** Integration of optically active materials into whispering gallery mode (WGM) cavities enables low-threshold laser emission. In contrast to their passive counterparts, the WGMs of these microlasers can be pumped and read out easily via free-space optics. The WGMs interact with the cavity environment via their evanescent field, and thus lend themselves to label-free bio-sensing. The detection limit of such sensors, given as the ratio of the resolution of the whole measurement system to the sensitivity of the WGMs, is an important figure of merit. In this work we show that the detection limit of polymeric microdisk lasers can be improved by more than a factor of seven by optimizing their radius and thickness. We use the bulk refractive index sensitivity, the magnitude of the sensor reaction towards refractive index changes of the bulk environment, to quantify the sensing performance and show that it can be enhanced while the spectral resolution is maintained. Furthermore, we investigate the effect of the size of the cavity on the quality factor and the lasing threshold in an aqueous environment, hence allowing optimization of the cavity size for enhanced sensor performance. For all considered quantities, numerically computed expectations are verified by experimental results.



**OCIS codes:** (140.4780) Optical resonators; (140.3948) Microcavity devices; (280.4788) Optical sensing and sensors.

## References and links

1. S. Arnold, M. Khoshsima, I. Teraoka, S. Holler, and F. Vollmer, "Shift of whispering-gallery modes in microspheres by protein adsorption," Opt. Lett. **28**(4), 272–274 (2003).
2. P. Michler, A. Kiraz, C. Becher, W. V. Schoenfeld, P. M. Petroff, L. Zhang, E. Hu, and A. Imamoglu, "A quantum dot single-photon turnstile device," Science **290**(5500), 2282–2285 (2000).
3. J. Pfeifle, A. Coillet, R. Henriet, K. Saleh, P. Schindler, C. Weimann, W. Freude, I. V. Balakireva, L. Larger, C. Koos, and Y. K. Chembo, "Optimally coherent Kerr combs generated with crystalline whispering gallery mode resonators for ultrahigh capacity fiber communications," Phys. Rev. Lett. **114**(9), 093902 (2015).
4. J. D. Swaim, J. Knittel, and W. P. Bowen, "Detection of nanoparticles with a frequency locked whispering gallery mode microresonator," Appl. Phys. Lett. **102**(18), 183106 (2013).
5. F. Vollmer, S. Arnold, and D. Keng, "Single virus detection from the reactive shift of a whispering-gallery mode," Proc. Natl. Acad. Sci. U.S.A. **105**(52), 20701–20704 (2008).
6. M. D. Baaske, M. R. Foreman, and F. Vollmer, "Single-molecule nucleic acid interactions monitored on a label-free microcavity biosensor platform," Nat. Nanotechnol. **9**(11), 933–939 (2014).
7. M. L. Gorodetsky, A. A. Savchenkov, and V. S. Ilchenko, "Ultimate Q of optical microsphere resonators," Opt. Lett. **21**(7), 453–455 (1996).
8. D. K. Armani, T. J. Kippenberg, S. M. Spillane, and K. J. Vahala, "Ultra-high-Q toroid microcavity on a chip," Nature **421**(6926), 925–928 (2003).
9. Z. Guo, H. Quan, and S. Pau, "Near-field gap effects on small microcavity whispering-gallery mode resonators," J. Phys. D Appl. Phys. **39**(24), 5133–5136 (2006).
10. H. Chandrahalim, S. C. Rand, and X. Fan, "Fusion of renewable ring resonator lasers and ultrafast laser

#283444 https://doi.org/10.1364/OE.25.007884
Journal © 2017 Received 13 Jan 2017; revised 19 Feb 2017; accepted 21 Feb 2017; published 28 Mar 2017

Optics EXPRESS

inscribed photonic waveguides," Sci. Rep. **6**, 32668 (2016).
11. A. L. Schawlow and C. H. Townes, "Infrared and optical masers," Phys. Rev. **112**(6), 1940–1949 (1958).
12. L. Yang, T. Lu, T. Carmon, B. Min, and K. J. Vahala, "A 4-Hz fundamental linewidth on-chip microlaser," in *CLEO, San Jose* (2007), pp. 4–5.
13. I. M. White and X. Fan, "On the performance quantification of resonant refractive index sensors," Opt. Express **16**(2), 1020–1028 (2008).
14. J. Hu, X. Sun, A. Agarwal, and L. C. Kimerling, "Design guidelines for optical resonator biochemical sensors," J. Opt. Soc. Am. B **26**(5), 1032–1041 (2009).
15. T. Reynolds, M. R. Henderson, A. François, N. Riesen, J. M. M. Hall, S. V. Afshar, S. J. Nicholls, and T. M. Monro, "Optimization of whispering gallery resonator design for biosensing applications," Opt. Express **23**(13), 17067–17076 (2015).
16. T. Grossmann, S. Schleede, M. Hauser, M. B. Christiansen, C. Vannahme, C. Eschenbaum, S. Klinkhammer, T. Beck, J. Fuchs, G. U. Nienhaus, U. Lemmer, A. Kristensen, T. Mappes, and H. Kalt, "Low-threshold conical microcavity dye lasers," Appl. Phys. Lett. **97**(6), 63304 (2010).
17. T. Wienhold, S. Kraemmer, S. F. Wondimu, T. Siegle, U. Bog, U. Weinzierl, S. Schmidt, H. Becker, H. Kalt, T. Mappes, S. Koeber, and C. Koos, "All-polymer photonic sensing platform based on whispering-gallery mode microgoblet lasers," Lab Chip **15**(18), 3800–3806 (2015).
18. T. Grossmann, M. Hauser, T. Beck, C. Gohn-Kreuz, M. Karl, H. Kalt, C. Vannahme, and T. Mappes, "High-Q conical polymeric microcavities," Appl. Phys. Lett. **96**(1), 013303 (2010).
19. T. Grossmann, T. Wienhold, U. Bog, T. Beck, C. Friedmann, H. Kalt, and T. Mappes, "Polymeric photonic molecule super-mode lasers on silicon," Light Sci. Appl. **2**(5), e82 (2013).
20. G. Gupta, W. H. Steier, Y. Liao, J. Luo, R. Dalton, and A. K.-Y. Jen, "„Modeling photobleaching of optical chromophores: light-intensity effects in precise trimming of integrated polymer devices," J. Phys. Chem. C **112**(21), 8051–8060 (2008).
21. U. Bog, F. Brinkmann, S. F. Wondimu, T. Wienhold, S. Kraemmer, C. Koos, H. Kalt, M. Hirtz, H. Fuchs, S. Koeber, and T. Mappes, "Densely packed microgoblet laser pairs for cross-referenced biomolecular detection," Adv Sci (Weinh) **2**(10), 1500066 (2015).
22. V. B. Braginsky, M. L. Gorodetsky, and V. S. Ilchenko, "Quality-factor and nonlinear properties of optical whispering-gallery modes," Phys. Lett. A **137**(7,8), 394–397 (1989).
23. A. Dupuis, N. Guo, B. Gauvreau, A. Hassani, E. Pone, F. Boismenu, and M. Skorobogatiy, ""Colorful" solid-core Bragg fibers guiding in the visible," Opt. Lett. **32**(19), 2882–2884 (2008).
24. F. P. Schäfer, ed., *Dye Lasers* (Springer, 1990).
25. T. Wienhold, S. Kraemmer, A. Bacher, H. Kalt, C. Koos, S. Koeber, and T. Mappes, "Efficient free-space read-out of WGM lasers using circular micromirrors," Opt. Express **23**(2), 1025–1034 (2015).
26. R. M. Waxler, D. Horowitz, and A. Feldman, "Optical and physical parameters of Plexiglas 55 and Lexan," Appl. Opt. **18**(1), 101–104 (1979).
27. D. Solimini, "Loss measurement of organic materials at 6328 Å," J. Appl. Phys. **37**(8), 3314–3315 (1966).

## 1. Introduction

In recent years whispering gallery mode (WGM) cavities have attracted a lot of attention in research due to their broad application opportunities including sensing [1], cavity quantum electrodynamics [2] and optical communications [3]. Especially in the field of label-free bio-sensing, WGM cavities feature great potential, which was proven by successful detection of, e.g., nanoparticles [4], viruses [5], proteins [1] and DNA [6]. WGMs occur when light is propagating along a curved dielectric interface and stand out due to remarkably low propagation losses, which can be exploited to realize microcavities with remarkably high quality factors. Importantly, WGMs exhibit an evanescent field interacting with the environment of the cavity, whereby the resonance conditions depend on the optical properties of the surrounding. Hence, the spectral position of the WGMs can serve as sensor signal to monitor minute refractive index changes or adsorption of molecular layers to the dielectric interfaces.

The phenomenon of WGMs has been studied in cavities of various geometries and materials. Prominent examples are silica spheres and toroids which exhibit extremely high quality factors up to $8 \times 10^9$ [7]. However, excitation and read-out of the WGMs in these cavities is often based on tapered fibers or prisms [8], thus requiring sophisticated equipment for precise alignment which limits practical applicability outside laboratory environments. Furthermore, the spectral position of the resonant modes is influenced by the external couplers which can disturb the actual signal [9].

Optics EXPRESS

These limitations can be overcome when optically active materials are integrated in the cavities enabling pumping and read-out of the WGMs via free-space optics. Recently, renewable ring resonator lasers, which can be read-out with an adjacent waveguide, have been realized [10]. Operating such WGM cavities in the lasing regime results in lasing modes of narrow linewidths [11,12], far below the resonance linewidth of the passive cavity, and often also below the resolution of the spectrometer used to characterize and read out the device.

One crucial parameter for evaluation of (bio)sensor performance is the detection limit which is given as the ratio of the system resolution to the sensitivity of the sensing element, which is the cavity in our case. Since for WGM lasers the resolution is usually limited by the spectrometer, a promising method to improve the detection limit is to enhance the sensitivity. An easily accessible sensitivity is the so-called bulk refractive index sensitivity (BRIS), which is defined as the magnitude of the spectral shift of the resonance upon changes in the refractive index of the surrounding. White *et al.* showed that the shift caused by molecules attaching to the cavity surface is proportional to the BRIS [13], i.e., the BRIS can be used to quantify the general sensing performance. The BRIS depends on the spatial overlap of the WGMs with the surrounding and hence strongly depends on the size and the refractive index of the cavity. Different approaches dealing with the design optimization of optical microcavities for sensing applications can be found in literature [13–15]. In [14], design guidelines for passive optical ring resonators are discussed. In [15], Reynolds *et al.* present a theoretical model for spherical cavities which allows to predict the sensing performance of cavities of different radius and refractive index. However, a systematic and experimentally confirmed analysis for optimization of the cavity size of WGM lasers has not yet been done.

In this paper, we present a theoretical and experimental investigation how the sensing performance of polymeric microdisk lasers is influenced by the cavity size. When using disk resonators instead of spheres, both the radius and the thickness of the cavity can be varied independently providing an additional degree of freedom. Additionally, microdisks are more sensitive towards changes in the environment than microspheres, due to the increased mode overlap with the environment at top and bottom of the disk. We investigate theoretically how the BRIS of dye-doped polymeric microdisk lasers can be enhanced by varying the radius and the thickness of the cavity, and we confirm the results by experiments. Furthermore, we investigate the influences of the size variation on the quality factor and the lasing threshold in aqueous environment. We also discuss the detection limit and compare the influence of noise on the resolution for passive and active WGM configurations.

## 2. Fabrication and methods

Our analysis uses dye-doped polymeric microdisk lasers. Polymeric cavities allow an easy integration of optical emitters and can be fabricated with a scalable low-cost fabrication process [16]. Furthermore, on-chip integration of the microdisk lasers is feasible and has already been demonstrated [17].

We fabricate polymeric microdisk cavities consisting of PMMA (poly(methyl methacrylate)) according to the procedure presented in [18]. In order to obtain WGM lasers, we add the laser dye pyrromethene 597 (PM597) to the photoresist (PMMA 950k) at a concentration of 25 µmol/g PMMA prior to fabrication. Stirring the solution of the dye and the photoresist for several hours ensures that the dye is dissolved properly. For fabrication of the disk cavities, the dye-doped PMMA is spin-coated onto a silicon wafer and disks are patterned via electron-beam lithography. Structuring with deep-UV lithography is also feasible but due to the varying disk radius, electron-beam lithography is preferred [17]. Subsequent isotropic etching with $XeF_2$ removes the silicon beneath the rim of the disks yielding microdisk cavities. By modifying the spin-coating speed or the lithography pattern, the thickness or the radius of the disk resonators can be varied. We fabricated disks with a fixed thickness of $d = 0.9$ µm and radii ranging from $R = 7.5$ µm to $R = 25$ µm and disks with

Optics EXPRESS

a fixed radius of $R$ = 25 µm and thicknesses between $d$ = 0.21 µm and $d$ = 0.9 µm. The thickness of the resulting microdisks was determined from SEM images with an accuracy of approximately 10%. Figure 1 depicts an SEM image of such a PMMA microdisk with a radius of $R$ = 8.75 µm and a thickness of $d$ = 0.9 µm standing on a silicon pedestal.

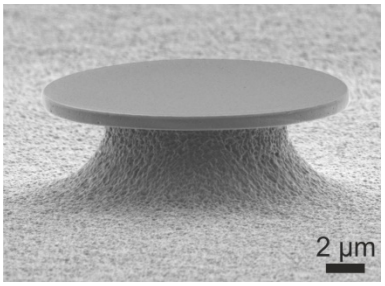


Fig. 1. SEM image of a microdisk cavity with a radius of $R$ = 8.75 µm and a thickness of $d$ = 0.9 µm.

For excitation and read-out of the microdisk lasers, a micro-photoluminescence (µ-PL) setup is used. A frequency-doubled Nd:$YVO_4$ laser emitting pulses with a pulse length of 10 ns and a repetition rate of 20 Hz at 532 nm is loosely focused on the sample. Typically, spot sizes of approximately three times the cavity diameter are used to ensure homogeneous illumination. The emitted light is collected with a microscope objective (50 × , NA = 0.42) and imaged onto a spectrometer equipped with a CCD camera with a spectral resolution of 33 pm. Usually exposure times of 2 s per spectrum were used. Further details on the µ-PL setup can be found in [19]. To enable experiments in aqueous environments, a fluidic chamber with inlet and outlet ports allowing an easy exchange of liquids is integrated into the optical setup. Figure 2 depicts a typical lasing spectrum of an excited microdisk, showing well separated lasing peaks on top of a fluorescence background due to spontaneous emission. The spectral distance between adjacent peaks, the so-called free spectral range, is determined to be 1.76 nm and fits well to the designed cavity radius of $R$ = 22.5 µm . Due to the evanescent field, the spectral position of the lasing modes is sensitive to changes in the environment and hence serves as sensor signal.

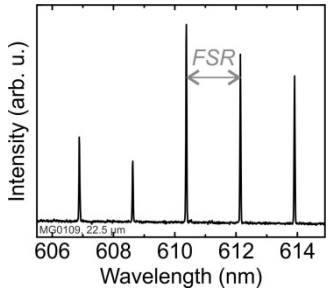


Fig. 2. Typical lasing spectrum of a microdisk cavity in aqueous environment. Different lasing modes separated by the free spectral range (FSR) serve as sensor signal. A pump fluence of 10 mJ/cm$^2$ was used to acquire this spectrum.

## 3. Polymeric microdisk lasers of varying size

We use the bulk refractive index sensitivity (BRIS) to evaluate the sensing performance of the cavities. The BRIS itself increases when the mode overlap of the WGMs with the environment increases. In the following we show that by reducing the size of microdisk lasers, the overlap of the WGMs with the environment and hence the BRIS can be enhanced. Furthermore, we investigate how other performance parameters, namely the Q-factor and the lasing threshold, are affected by the size variation.

Optics EXPRESS

### 3.1 Bulk refractive index sensitivity

For BRIS measurements, the polymeric WGM lasers were placed inside the fluidic chamber filled with water and pumped above lasing threshold. The pump fluence was in the range between 7.5 mJ/cm$^2$ and 23 mJ/cm$^2$ depending on the lasing threshold of the individual microdisks. Solutions of different refractive indices were prepared by mixing water and glycerol at different ratios. Lasing spectra of the microdisks were continuously acquired while the fluidic chamber was alternately filled with pure water and the water-glycerol mixtures. The filling was carried out manually by connecting syringes to the inlet port of the fluidic chamber and carefully injecting the different solutions. The flow rate was not explicitly measured, but can be estimated to be roughly 0.1 ml/s. For each solution fifteen spectra were acquired. The spectral positions of the lasing peaks were determined by fitting Gaussian functions to the data. Figure 3 shows a typical example of a BRIS measurement; Fig. 3(a) depicts exemplary the spectral shift of one lasing mode over time and Fig. 3(b) the spectral shift as a function of the refractive index change of the environment. The slope of the linear regression yields the BRIS. During BRIS measurements bleaching of the dye molecules occurs which can lead to a blue-shift of the lasing modes since the refractive index of the dye is lowered [20]. If this behavior is observed the water baseline is used for correction; when biosensing is performed referencing techniques can be applied. Hence, the more important aspect is the lifetime of the lasing modes, which exceeded 150 spectra for all investigated disks (with exception of the ones with a radius of $R$ = 7.5 µm).

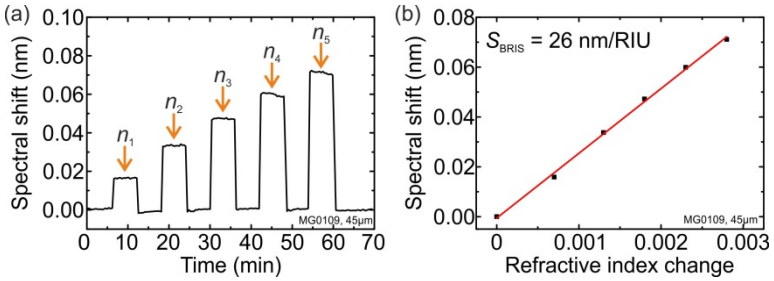


Fig. 3. Example of a typical BRIS measurement. (a) Spectral shift of one lasing mode over time, when the microdisk is alternately surrounded by pure water (base line) and water-glycerol mixtures with increasing refractive indices ($n_1$ = 1.3336, $n_2$ = 1.3342, $n_3$ = 1.3347, $n_4$ = 1.3352, $n_5$ = 1.3357 and $n_{water}$ = 1.3329). (b) BRIS is obtained from the slope of a linear fit (red) applied to the measured spectral shift (black square). A pump fluence of 10 mJ/cm$^2$ was used.

BRIS measurements were conducted for microdisk lasers of varying radius and thickness. For each parameter configuration, multiple microdisk lasers were investigated. In order to obtain theoretical predictions for the BRIS values we conducted simulations based on the finite element method (FEM). To this end, we used the software JCMSuite from JCMwave to determine the eigenmodes for a given cavity geometry. When exploiting the rotational symmetry of the cavities, numerically efficient 2D simulations can be performed. In order to simulate the BRIS, the refractive index of the environment was varied, resulting in spectrally shifted eigenmodes. Simulations were performed for fundamental transverse electric (TE) and transverse magnetic (TM) modes. For TE modes the electric field is dominantly polarized in the plane of the microdisk while for TM modes the dominant component of the electric field is out of plane. Since in experiments the lasing emission occurred at wavelengths between 560 nm and 630 nm, simulations were performed for these two confining wavelengths. For the given configuration of the µ-PL setup, the detection path is perpendicular to the plane of the microcavity. Thus, only non-polarized scattered light is collected making distinction between TE and TM modes difficult.

Optics EXPRESS

Figure 4 displays the simulation results of the BRIS values as well as the experimental data. The values are in good agreement and, as expected, an enhancement of the BRIS with decreasing radius and thickness of the microdisks is observed. Concerning the radius, a decrease leads to a maximum measured BRIS value of about 60 nm/RIU for disks with a radius of $R$ = 7.5 µm and a thickness of $d$ = 0.9 µm. For disks with even smaller radii, no lasing emission in aqueous environment could be achieved due to high radiation losses. For microdisk lasers with a constant thickness of $d$ = 0.9 µm [data shown in Fig. 4(a)] different BRIS values for the same cavity radius were observed (see e.g. $R$ = 17.5 µm). We attribute these different values to different cavity modes. The values plotted in red are assumed to correspond to fundamental modes, whereas the data points in black most likely arise from higher-order modes with more than one field maximum along the radial or the $z$-direction. The basis for this assumption is that simulations yield higher BRIS values for higher order modes than for fundamental modes due to the higher field overlap with the environment. When the thickness of the disk cavities is modified [see Fig. 4(b)], BRIS values exceeding 150 nm/RIU were measured for microdisk lasers with a thickness of $d$ = 0.21 µm. This corresponds to an enhancement of more than a factor of 7.5 compared to the polymeric microgoblet lasers previously used for bio-sensing measurements [21].

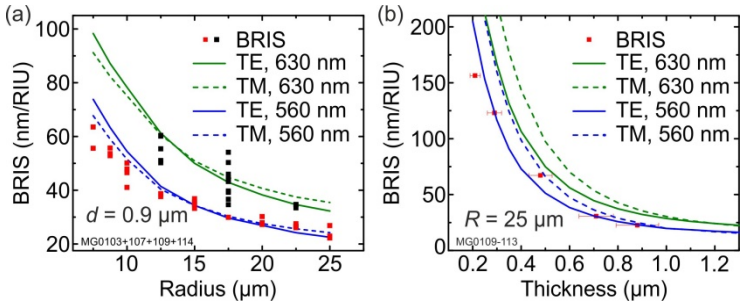


Fig. 4. BRIS values for microdisks of varying radius (a) and varying thickness (b). With decreasing radius and thickness, an enhancement of the BRIS is observed due to higher overlap of the WGMs with the environment. The results from FEM simulations (green and blue lines) are in good agreement with the measured data. Since the lasing wavelength range during the experiments decreased with decreasing radius or thickness, simulations were performed for confining wavelengths of 560 nm and 630 nm. Data points in red are attributed to fundamental modes while the black data points in (a) are attributed to higher order modes. In (a) each data point corresponds to a single measurement while in (b) the mean value is shown since only fundamental modes were present.

### *3.2 Quality factor and lasing threshold*

Besides the BRIS also the Q-factor and the lasing threshold are important performance parameters of WGM sensors. We determined both quantities for the polymeric WGM lasers of varying radius and thickness. All measurements were conducted in aqueous environment since biosensing experiments usually deal with liquids. The total Q-factor $Q$ is limited by several loss mechanisms, namely absorption, radiation and scattering [22],

$$Q^{-1} = Q_{\text{abs}}^{-1} + Q_{\text{rad}}^{-1} + Q_{\text{scat}}^{-1} \tag{1}$$

$Q_{\text{abs}}$ denotes the Q-factor only considering absorption losses, $Q_{\text{rad}}$ the radiation-limited Q-factor and $Q_{\text{scat}}$ the Q-factor due to scattering losses. PMMA exhibits low absorption in the visible wavelength range, hence absorption limited Q-factors up to $10^8$ are feasible [22, 23]. Scattering losses arise from imperfections of the cavity surface. Their magnitude is difficult to predict theoretically since time-consuming full 3D simulations with high computational costs would be required. However, when working in aqueous environment, the refractive index contrast between cavity material and surrounding is rather small making radiation the

Optics EXPRESS

dominating loss mechanism when the cavity size falls below certain values. With FEM simulations, the Q-factor due to radiation losses can be easily determined via

$$Q_{\mathrm{rad}} = \frac{\omega_{\mathrm{real}}}{2\omega_{\mathrm{imag}}} \tag{2}$$

where $\omega_{\mathrm{real}}$ and $\omega_{\mathrm{imag}}$ denote the real and the imaginary part of the complex resonance frequency of the calculated eigenmode. Hence, in the following the radiation-limited Q-factor will serve as theoretical value to quantify resonator losses. For Q-factor measurements, a tunable external-cavity diode laser emitting at wavelengths around 635 nm with a linewidth of less than 0.4 fm was coupled to a tapered fiber which was brought in close proximity to the microdisk cavity. The transmission through the fiber taper was recorded with a photo diode. From the linewidth of the resonance dips in the transmission spectrum, the Q-factor was extracted. Figure 5 depicts both Q-factors only considering radiation losses determined from FEM simulations and experimental results for microdisk cavities of varying radius and a fixed thickness of $d$ = 0.9 µm and varying thickness and a fixed radius of $R$ = 25 µm. For small radii, theoretical and experimental values are in good agreement, indicating that radiation losses are indeed the dominating loss mechanism. When the radius exceeds 12.5 µm, the experimentally measured Q-factors are smaller than the simulated ones. In this range, scattering losses which were not considered in the simulations become the dominant loss mechanism. For disks of varying thickness and constant radius [$R$ = 25 µm, see Fig. 5(b)] a similar trend was observed. Q-factor measurements for microdisks of thicknesses below $d$ = 0.35 µm were not possible since extremely thin fibers would be required to achieve appropriate phase matching. However, for a thickness of $d$ = 0.35 µm the experimental Q-factor agrees well with simulation results indicating that the radiation limited regime is reached. For thicknesses exceeding $d$ = 0.35 µm, the measured Q-factors are lower than the values from simulations again showing that in this range scattering is again the dominating loss channel. The measured Q-factors in this range saturate at values of approximately $10^5$.

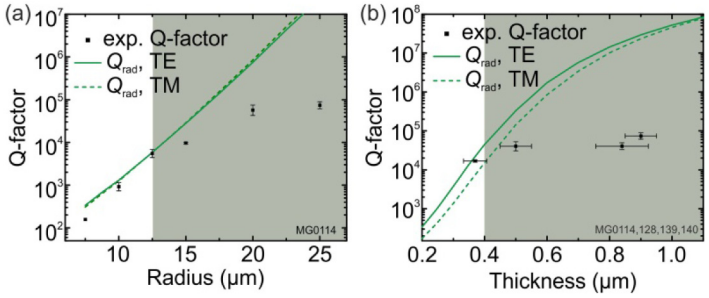


Fig. 5. Q-factors of microdisk cavities of varying radius and constant thickness ($d$ = 0.9 µm) (a) and varying thickness and constant radius ($R$ = 25 µm) (b) in aqueous environment – experimentally determined values (black data points) and simulation results of the radiation-limited Q-factor (green). For small radii and thicknesses, radiation is the dominating loss channel whereas, for larger radii and thicknesses scattering losses limit the Q-factor (area marked in grey). There are no errors bars for the Q-factors of disks with a radius of $R$ = 7.5 µm in (a) since only one resonator was investigated.

For operation of our microdisk lasers, the lasing threshold which depends on the Q-factor is an important figure of merit as it defines the required power of the pump source. Furthermore, the lasing threshold also affects the operation lifetime of the microdisk lasers since higher pump energies lead to increased bleaching of the dye molecules. According to [24], the lasing threshold can be calculated by

Optics EXPRESS

$$P_{\mathrm{th}} = \frac{\gamma h c_0}{\tau \lambda_{\mathrm{p}} \sigma_{\mathrm{a}}^2(\lambda_{\mathrm{p}}) n_{\mathrm{t}} d} \tag{3}$$

where $\gamma$ is the minimum fraction of excited dye molecules required for lasing, $h$ is Planck's constant, $c_0$ is the vacuum speed of light, $\tau$ is the fluorescence lifetime of the dye molecule, $\sigma_{\mathrm{a}}^2(\lambda_{\mathrm{p}})$ is the quadratic absorption cross section at the pump wavelength $\lambda_{\mathrm{p}}$, $n_{\mathrm{t}}$ is number density of dye molecules, and $d$ is the thickness of the disk. Since the minimum fraction of excited molecules $\gamma$ depends on the Q-factor $Q$ of the cavity, the lasing threshold is influenced by the Q-factor,

$$P_{\mathrm{th}} \propto \gamma(\lambda) \geq \frac{\frac{2\pi n}{\lambda Q n_{\mathrm{t}}} + \sigma_{\mathrm{a}}(\lambda)}{\sigma_{\mathrm{a}}(\lambda) + \sigma_{\mathrm{e}}(\lambda)} \tag{4}$$

Here, $n$ denotes the refractive index of the cavity, $\lambda$ is the wavelength and $\sigma_{\mathrm{a}}(\lambda)$ and $\sigma_{\mathrm{e}}(\lambda)$ denote the absorption and emission cross section, respectively. The absorption and emission cross section can be determined by [24]

$$\sigma_{\mathrm{a}}(\lambda) = 0.385 \cdot 10^{-20} \epsilon(\lambda), \tag{5}$$

$$\sigma_{\mathrm{e}}(\lambda) = \frac{\lambda^4 f(\lambda) \Phi_{\mathrm{f}}}{8\pi c_0 n^2 \tau} \tag{6}$$

where $\epsilon(\lambda)$ denotes the extinction coefficient in liter/(mol · cm), $f(\lambda)$ denotes the normalized photoluminescence spectrum and $\Phi_{\mathrm{f}}$ the fluorescence quantum yield. All the quantities required to calculate the lasing threshold were obtained from respective measurements performed on dye-doped PMMA films spin-coated on glass substrates.

For measurements of the lasing threshold, the µ-PL setup described above was used. Spectra were acquired for varying excitation energies. The lasing thresholds were obtained from so-called input-output curves where the integrated intensity of the lasing modes after subtraction of the fluorescence background is plotted versus the deposited pump energy. [see Fig. 6(a)]. When the pump energy exceeds the energy necessary for lasing, the slope of the output curve increases and the kink in this plot yields the lasing threshold. Figures 6(b) and 6(c) depict the experimentally determined lasing thresholds in aqueous environment as well as the expected values calculated with Eq. (3). It is obvious that both smaller radii and thicknesses lead to increased lasing thresholds due to reduced Q-factors and in the latter case also since the thickness directly enters the threshold (see Eq. (4). The calculated lasing thresholds show the same trend as the measured data. Quantitatively deviations can be observed but the agreement is acceptable when taking into account how many quantities afflicted with uncertainties are required for calculating the threshold.

In the plots in Fig. 6, two regions can be distinguished: When the Q-factor is still in the scattering-limited regime ($R$ > 12.5 µm or $d$ > 0.4 µm), the threshold only increases slightly and remains within an acceptable range for applications. For radii below $R$ = 12.5 µm or thicknesses below $d$ = 0.4 µm, the increase in threshold becomes more severe since the Q-factors exhibit a decrease due to continuously increasing radiation losses. The optimal cavity dimensions with significantly enhanced BRIS but acceptable lasing thresholds are thus $R$ = 12.5 µm and $d$ = 0.4 µm, corresponding to BRIS values of approximately 40 nm/RIU and 75 nm/RIU respectively, see Fig. 4. The comparison of the results for the microdisks of reduced radius and thickness shows that thinner cavities can achieve higher BRIS values while maintaining comparably low lasing thresholds (When the pump energies per resonator are

Optics EXPRESS

considered, the thresholds are still in the order of few nJ). Hence, reducing the thickness brings higher benefits in sensitivity than reducing the radius of the cavity.

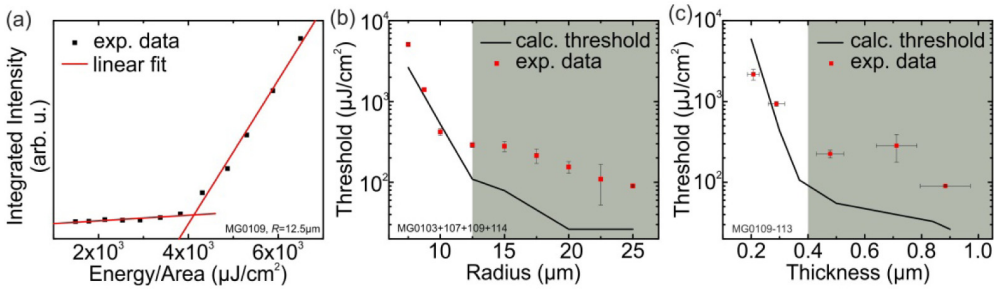


Fig. 6. (a) Typical input-output curve to determine the lasing threshold. (b) and (c) Calculated and measured lasing thresholds in aqueous environment of microdisk cavities of varying radius and thickness. With decreasing radius and thickness the lasing threshold increases due to lower Q-factors and for the latter also due to the reduced thickness of the cavity. The grey area marks the regime where the scattering losses limit the Q-factor.

### *3.3 Detection limit*

Besides the sensitivity $S$, the resolution $R$ of the system also plays an important role for applications in sensing. The ratio of these quantities corresponds to the detection limit, which represents the lowest refractive index change in the surrounding which can be detected [13]

$$DL = \frac{R}{S} \tag{7}$$

The resolution denotes the minimum resolvable spectral shift which can be detected and is given as $R = 3\sigma$ with $\sigma$ denoting the total noise variance. According to White *et al.*, two different kinds of noise have to be considered: amplitude noise and spectral noise [13].

For WGM lasers the resolution of the system is sustained upon size reduction since neither amplitude noise nor spectral noise increases. Hence, the enhancement in sensitivity directly leads to an improvement of the detection limit. In the following we discuss how the different noise sources are influenced by the size variation of the microdisk cavities. Furthermore, we comment on the differences between WGM lasers and passive WGM cavities.

Amplitude noise refers to cumulative noise added to the complete recorded spectrum [13]. It originates from, e.g., thermal noise or shot noise of the photodetector or intensity fluctuations of the tunable laser – the latter only playing a role when the cavities are operated in the passive regime. Since for WGM lasers several pump pulses (typically 40) contribute to one acquired spectrum, power fluctuations of the pump laser average and can be neglected. Amplitude noise leads to deviations in the central spectral position of the peak function fitted to the data. Based on Monte Carlo simulations, White *et al.* showed that the variance in the spectral position of the cavity mode due to amplitude noise is proportional to the linewidth of the mode and inversely proportional to the fourth-order root of the signal to noise ratio (SNR), relating the peak height above background to the amplitude noise [13]. For passive cavities where the WGMs are typically read out with a tunable laser or a prism, a reduction of the Q-factor directly leads to a broader measurable linewidth and hence an increased noise variance due to amplitude noise. For microdisk lasers, the measurable linewidth is usually limited by the resolution of the spectrometer. In our experiments, the measurable linewidth of the lasing peaks remained constant at the value given by the resolution of the spectrometer for the cavities with radii $R > 7.5$ µm and for all investigated thicknesses. Thus, in contrast to passive WGM cavities, the lower Q-factors did not lead to an increased noise variance due to amplitude noise.

Optics EXPRESS

The increase in lasing threshold for cavities of reduced sizes might result in lower heights of the lasing peaks and affect the SNR of the peak height above fluorescence background to the amplitude noise. However, this can be compensated by higher deposited excitation energies. Moreover, the height of the lasing peaks also depends on the amount of emitted laser light actually reaching the spectrometer and the CCD camera attached. By redirecting the light emitted in the plane of the microdisk to the spectrometer, the peak height of the lasing modes can be increased compared to case of collecting the light scattered perpendicular to the disk plane. Previously, we have shown the successful integration of conical mirrors around the cavities leading to an enhancement of the height of the lasing peak above fluorescence background by a factor of almost ten in air [25]. In aqueous environment, an even higher signal enhancement is expected since more radiation light escapes from the cavity modes due to the lower refractive index contrast of the cavity material and the environment. In addition to the simple excitation and read-out, this efficient method to lower the influence of amplitude noise on the system resolution is a further benefit of microdisk lasers compared to passive systems. An increased lasing threshold also effectuates the lifetime of the microdisks due to the higher required pump fluences. However for all investigated disks (except for the ones with a radius of $R$ = 7.5 µm) the lifetime of the lasing modes was sufficient to perform BRIS measurements where at least 150 spectra were acquired.

Thermally induced spectral noise describes fluctuations of the spectral position of the WGMs caused by temperature variations. It mainly depends on the temperature stability of the setup and on the thermo-optic coefficients and the expansion coefficients of the cavity material and the surrounding. For PMMA, changes in the refractive index are the dominant source of thermally induced spectral noise in the investigated spectral region [26]. Upon size reduction of the cavities the WGMs show an increased overlap with the surrounding. Since water exhibits a lower thermo-optic coefficient than PMMA [26] [27], a decrease in thermally induced spectral noise for increasing overlap of the modes with the environment is expected.

## 4. Summary and conclusion

In this paper we showed that the BRIS of WGM microdisk lasers can be enhanced by reducing both the radius and the thickness of the cavity. Simulation and experimental results were compared and found to be in good agreement. Reducing the size of the microdisk lasers leads to an increased overlap of the resonant modes with the environment and thus to an increased BRIS. Enhancement factors exceeding 7.5 have been found. The enhancement in the BRIS is accompanied by a reduction of the Q-factor, resulting in an increase in lasing threshold. However, in contrast to passive WGM cavities, the resolution is not affected by the reduced Q-factor as usually the spectral resolution of the spectrometer or thermally induced spectral noise is the bottleneck which is rather constant. Hence, the enhanced sensitivity directly leads to an improved detection limit.

When comparing the results of microdisks of reduced radius or thickness also taking simulation results into account, we find BRIS enhancement by thickness reduction to be more efficient. Taking also the lasing threshold into account, optimum results are achieved for disk thicknesses around $d = 0.4$ µm. In this case the Q-factor is still in the scattering-limited regime and hence the increase in lasing threshold is small. The microlasers of reduced thickness can be further optimized by using a thermal reflow step at the end of the fabrication process as presented in [18]. During the reflow, the surface of the microdisks is smoothened and the disks are converted into microgoblets. The smoother surface reduces scattering losses which leads to higher Q-factors – hence lower lasing thresholds could be achieved while maintaining the high sensitivity.

Optics EXPRESS

## Acknowledgments

S. K. thanks the Carl Zeiss foundation for financial support. S. F. W. acknowledges financial support from the German states graduate fund (Landesgraduiertenförderung). S. K., T. S, S. F. W. and C. K. are/were pursuing their Ph.D. within the Karlsruhe School of Optics and Photonics (KSOP) and acknowledge continuous support.